Correlation of Microstructure with Mechanical Properties of Zr-Based Amorphous Matrix Composite Reinforced with Tungsten Continuous Fibers and Ductile Dendrites

CHANG-YOUNG SON, GYEONG SU KIM, SANG-BOK LEE, SANG-KWAN LEE, HYOUNG SEOP KIM, HOON HUH, and SUNGHAK LEE

A Zr-based amorphous matrix composite reinforced with tungsten continuous fibers in an amorphous LM2 alloy matrix containing ductile β dendrites was fabricated without pores or defects by the liquid pressing process, and its tensile and compressive properties were examined in relation with microstructures and deformation mechanisms. Overall, 68 vol pct of tungsten fibers were distributed in the matrix, in which 35 vol pct of β dendrites were present. The LM2 composite had the greatly improved tensile strength and elastic modulus over the LM2 alloy, and it showed a stable crack propagation behavior as cracks stopped propagating at the longitudinal cracks of tungsten fibers or ductile β dendrites. According to the compressive test results, fracture did not take place at one time after the yield point, but it proceeded as the applied loads were sustained by fibers, thereby leading to the maximum strength of 2432 MPa and plastic strain of 16.4 pct. The LM2 composite had the higher strength, elastic modulus, and ductility under both tensile and compressive loading conditions than the tungsten-fiber-reinforced composite whose matrix did not contain β dendrites. These distinctively excellent properties indicated a synergy effect arising from the mixing of amorphous matrix and tungsten fibers, as well as from the excellent bonding of interfaces between them.

DOI: 10.1007/s11661-012-1250-1

I. INTRODUCTION

PLASTIC zones in monolithic amorphous alloys are hardly observed under tensile or compressive loading because the plastic deformation is concentrated on highly localized shear bands.[1–4] This is why monolithic amorphous alloys show stress–strain curves observed in typically brittle materials such as ceramics, and their plastic strain ranges a couple of percent even under compressive loading.[5,6] To improve their ductility, intensive studies on fabrication of amorphous matrix composites have been performed by dispersing ductile crystalline particles, phases, or fibers.[7–17] For example, a Zr-based amorphous alloy containing ductile dendrites of crystalline β phases (structure, body-centered cubic [bcc]), *i.e.*, an LM2 alloy (commercial brand name of the Liquidmetal Technologies, Lake Forest, CA; composition $Zr_{56.2}Ti_{13.8}Nb_{5.0}Cu_{6.9}Ni_{5.6}Be_{12.5}$ at. pct) shows the improved ductility by the formation of deformation bands at dendrites and multiple shear bands in the amorphous matrix.[18,19]

Recently, a fabrication method of amorphous matrix composites reinforced with continuous metallic fibers, *i.e.*, a liquid pressing process, was developed to improve simultaneously the strength and ductility of amorphous alloys.[20,21] Because this process uses a low pressure near to the theoretically required minimum loading pressure, the crystallization of the amorphous matrix can be prevented or minimized by rapid cooling of the amorphous melt. It also has the advantages of complete infiltration of the melt inside the fiber because of the application of low hydrostatic pressure and elimination of pores formed by contraction during solidification. By using this process, Lee *et al.*[22] fabricated an amorphous matrix composite reinforced with tungsten continuous fibers in a matrix of a monolithic Zr-based amorphous alloy, *i.e.*, an LM1 alloy (commercial brand name of the Liquidmetal Technologies; composition: $Zr_{41.2}Ti_{13.8}Cu_{12.5}Ni_{10.0}Be_{22.5}$ at. pct). Its strength was improved as tungsten fibers with very high strength and elastic modulus took over a considerable amount of applied loads in the area where cracks were formed, but the ductility was not enhanced much even under the compressive loading condition. This insufficient ductility might be caused by the mismatch of tungsten fibers and

CHANG-YOUNG SON, formerly Postdoctoral Research Associate, Center for Advanced Aerospace Materials, Pohang University of Science and Technology, Pohang 790-784, Korea, is now Senior Researcher, Next Generation Products Research Group, Technical Research Laboratories, POSCO, Pohang 790-300, Korea. GYEONG SU KIM, Research Assistant, and HYOUNG SEOP KIM, Professor, are with the Department of Materials Science and Engineering, Pohang University of Science and Technology, Pohang, 790-784, Korea. SANG-BOK LEE and SANG-KWAN LEE, Senior Researchers, are with the Composite Materials Laboratory, Korea Institute of Materials Science, Chanwon 541-331, Korea. HOON HUH, Professor, is with the Department of Mechanical Engineering, Korea Advanced Institute of Science and Technology, Daejeon 350-701. Korea. SUNGHAK LEE, Professor, is with the Center for Advanced Aerospace Materials and Department of Materials Science and Engineering, Pohang University of Science and Technology. Contact e-mail: shlee@postech.ac.kr

Manuscript submitted September 26, 2011.
Article published online July 4, 2012

amorphous matrix whose strengths are very high without ductility.

Therefore, to improve the strength, elastic modulus, and ductility of the tungsten-fiber-reinforced amorphous matrix composite, the modified combination of tungsten fibers and other amorphous alloy was suggested in the current study. An amorphous matrix composite, whose matrix was an LM2 alloy, was fabricated by the liquid pressing process. Tungsten continuous fibers that have high melting temperature, strength, and thermal stability inside the melted matrix were used for reinforcements.[8,23–26] Microstructures of the fabricated composite were analyzed, and the tensile and compressive properties were evaluated. Deformation and fracture mechanisms were analyzed by observing deformed areas of the fractured composite specimens under tensile and compressive loading conditions. The results were then compared with those of the LM2 alloy and the tungsten-fiber-reinforced amorphous composite whose matrix was an LM1 alloy.

II. EXPERIMENTAL

An LM2 alloy and tungsten fibers were used as a matrix and reinforcements of the Zr-based amorphous matrix composite, respectively. Representative physical properties of the LM2 alloy and tungsten fibers, together with the LM1 alloy, are summarized in Table I.[22] Scanning electron micrographs of tungsten fibers and LM2 alloy are shown in Figures 1(a) and (b), respectively. The diameter of tungsten fibers is approximately 100 μm (Figure 1(a)). A dendritic structure of crystalline β phases is well developed in the LM2 alloy. This structure was formed as β phases were precipitated directly from the melt.[27,28] β dendrites are relatively evenly distributed in the amorphous matrix, and their size and volume fraction are approximately 20 μm and 35 pct, respectively.

Figure 2 shows a schematic diagram of the liquid pressing process used to fabricate the amorphous matrix composites. The inner size of the mold is 60 × 25 × 6 mm. A preform of tungsten fibers, together with LM2 alloy plates, were inserted into the mold, degassed, and vacuumed. The mold, inside which LM2 alloy plates were placed, was heated to 1143 K (870 °C) and held for 5 minutes to melt the interior LM2 alloy plates sufficiently, and then it was pressed under a pressure of 10 MPa. This pressing was accompanied with water cooling to form amorphous phases readily in the matrix.

The fabricated composite was sectioned; polished; etched in a solution of 70 mL H_2O, 25 g CrO_3, 20 mL HNO_3, and 2 mL HF; and observed by a scanning electron microscope (SEM; model JSM-6330F; JEOL Ltd., Tokyo, Japan). Volume fractions of tungsten fibers and crystalline β dendrites in the matrix were measured by an image analyzer. The amorphous forming properties of the LM2 alloy and composite were analyzed by a

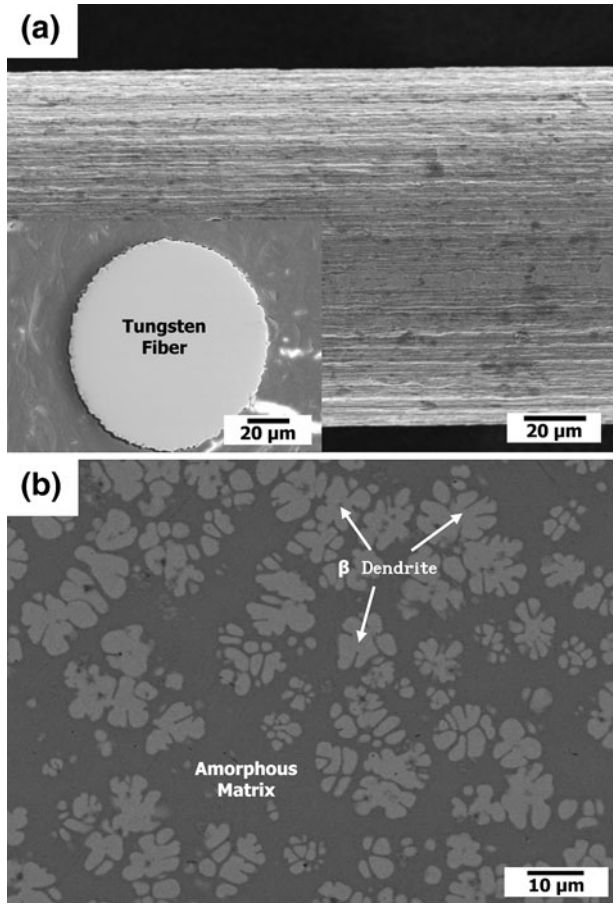

Fig. 1—SEM micrographs of (*a*) tungsten continuous fibers and (*b*) Zr-based amorphous LM2 alloy.

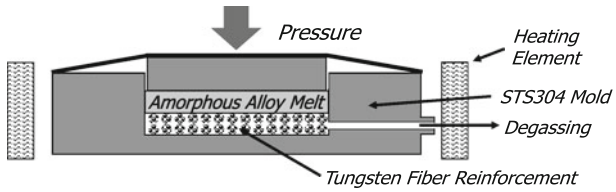

Fig. 2—Schematic diagram of the liquid pressing process.

Table I. Physical and Mechanical Properties of the LM1 Alloy, LM2 Alloy, and Tungsten Fiber

Property	LM1 Alloy	LM2 Alloy	Tungsten Fiber
Diameter (μm)	—	—	100
Density (g/cm^3)	6.1	6.3	19.3
Melting temperature, K (°C)	993 (720)	1005 (732)	3643 (3370)
Thermal expansion coefficient (10^{-6}/K)	8.5	10.2	4.6

differential scanning calorimeter (DSC; model DSC-7; Perkin-Elmer, Waltham, MA) at a heating rate of 20 K/min.

Plate-type tensile specimens with a gage length of 8 mm, a width of 2 mm, and a thickness of 1.5 mm were prepared and tested at room temperature at a strain rate of 1.5×10^{-4} s^{-1}. Because the tensile specimen size was very small to attach a strain gage, the precise measurement of strain was difficult. During the tensile test, thus, strains were measured by a vision strain gauge system (model ARAMIS v6.1; GOM Optical Measuring Techniques, Braunschweig, Germany), which could detect three-dimensional coordinates of the deforming specimen surface on the basis of the digital image process delivering three-dimensional displacement and strain. This ARAMIS system recognized the surface structure of the measuring specimen in digital camera images and allocated coordinates to image pixels. After or during the deformation of the measuring specimen, digital camera images were recorded. Tensile stress–strain curves could be drawn by matching time–strain values obtained from this ARAMIS system with time–strain curves experimentally obtained from a universal testing machine. The composite was machined into rectangular bar specimens of $3 \times 3 \times 5$ mm in size, and room-temperature compression tests were conducted on these specimens at a strain rate of 5.6×10^{-4} s^{-1}. Tensile and compressive testing was performed by a universal testing machine (model 5567; Instron Corporation, Norwood, MA) with capacity of 3000 kg using three specimens at least at each testing condition. To investigate the tensile and compressive deformation behaviors, the deformed area of the fractured specimen was observed by an SEM.

III. RESULTS

A. *Microstructure*

DSC curves of the LM2 alloy and its composite are shown in Figure 3. The glass transition temperatures (T_g) of the alloy and composite are 620 K (347 °C) and 622 K (349 °C), respectively. This observation implies that characteristics of the amorphous matrix are hardly changed during the liquid pressing process. The crystallization temperature (T_x) of the composite is 658 K (385 °C), which is lower by 4 K than that of the LM2 alloy. These DSC results indicate that the amorphous matrix is hardly crystallized because of the high thermal stability of tungsten fibers.

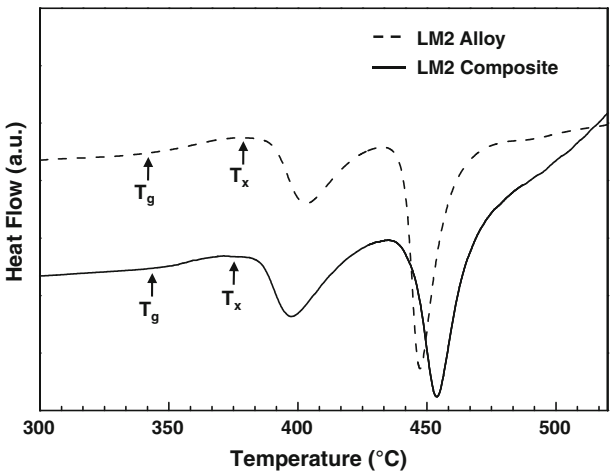

Fig. 3—DSC curves of the LM2 alloy and tungsten-fiber-reinforced LM2 composite.

Figures 4(a) and (b) are SEM micrographs of the Zr-based amorphous matrix composite reinforced with tungsten fibers. Tungsten fibers are homogeneously distributed in the matrix, and their volume fraction is 68 pct (Figure 4(a)). β dendrites are found in the matrix, and their fraction is approximately 35 pct inside the matrix (Figure 4(b)), which is similar to that in the LM2 alloy (Figure 1(b)). Other crystalline phases are hardly observed as the crystallization did not occur because of high thermal stability of tungsten fibers. Pores or defects formed by misinfiltration or reaction products formed by interfacial reaction at fiber/matrix interfaces are not observed.

B. *Tensile Properties of Tungsten-Fiber-Reinforced Composite*

Figure 5(a) shows tensile and compressive stress–strain curves of the LM2 alloy and tungsten-fiber-reinforced

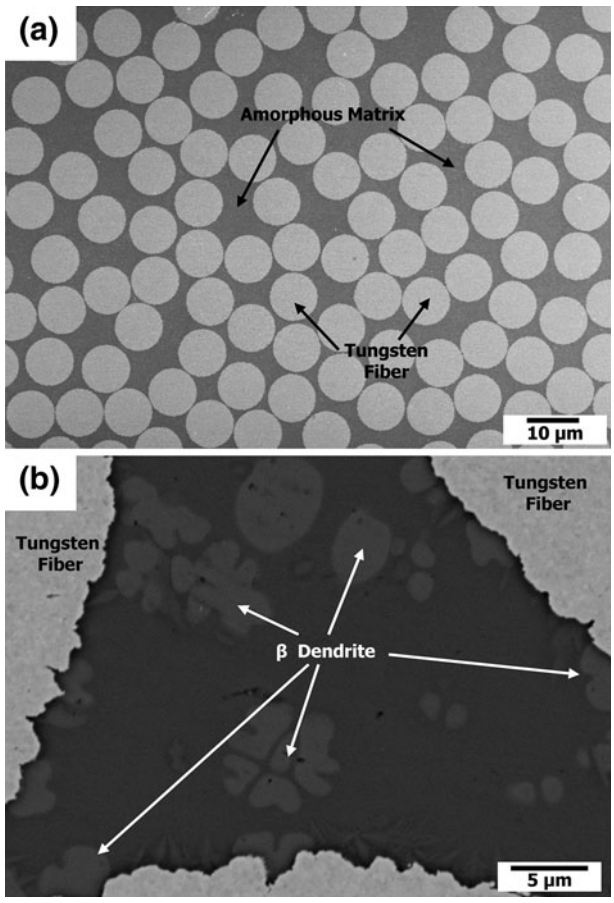

Fig. 4—(*a* and *b*) SEM micrographs of the tungsten-fiber-reinforced LM2 composite.

composite (hereafter referred to as LM2 composite). These tensile test results, together with tensile test results of tungsten fibers,[22] are summarized in Table II and are also compared with those of the LM1 alloy and tungsten-fiber-reinforced composite whose matrix is the LM1 alloy (hereafter referred to as LM1 composite).[22]

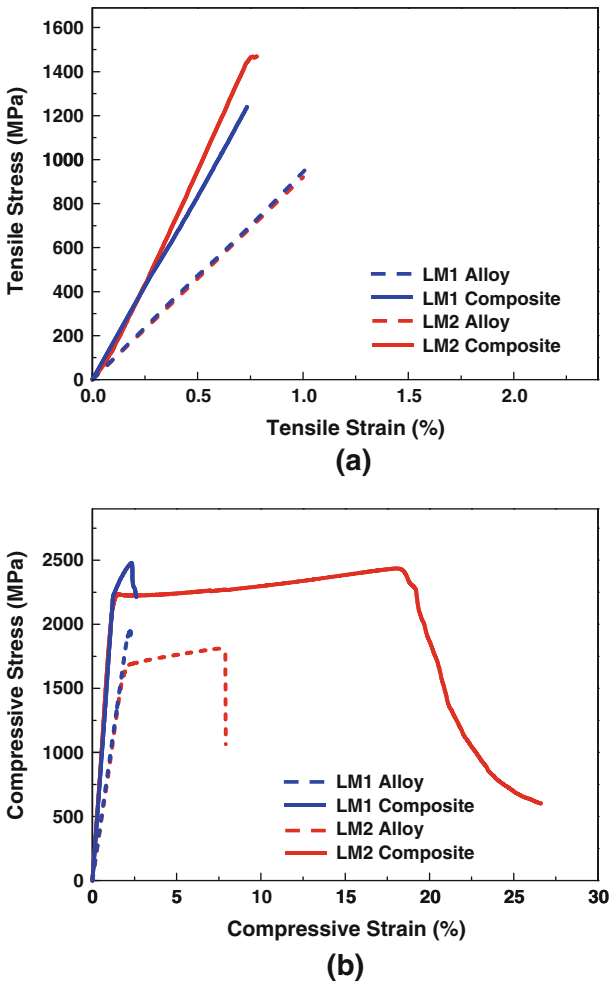

Fig. 5—(*a*) Tensile and (*b*) compressive stress–strain curves of the LM2 alloy and tungsten-fiber-reinforced LM2 composite. Curves of the LM1 alloy and tungsten-fiber-reinforced LM1 composite are also included for a comparison.

The LM2 alloy has the tensile strength of 927 MPa, and it hardly shows the ductility. The tensile strength of the LM2 composite is 1456 MPa, which is higher by approximately 530 MPa than that of the LM2 alloy, but the tensile elongation is very small at 0.03. The elastic modulus of the LM2 composite is very high at 195 GPa, which is twice as high as that of the LM2 alloy. The increase in tensile strength and elastic modulus is associated mainly with the containment of high-strength, high-stiffness tungsten fibers (tensile strength = 2395 MPa, elastic modulus = 411 GPa). When the LM2 composite is compared with the LM1 composite, the tensile strength is higher by approximately 220 MPa.

Figures 6(a) through (e) show SEM micrographs of the side region and fractograph of the tensile specimen of the LM2 composite. The fracture surface is almost perpendicular to the tensile direction in general, and fiber pull-outs are not observed (Figures 6(a) and (b)). This finding implies a very strong fiber/matrix interfacial bonding. Some fibers beneath the fracture surface are longitudinally cracked, and transverse cracks are also found in areas distant (approximately 100 μm) from the fracture surface as marked by arrows in Figure 6(b). Multiple shear bands are formed in the amorphous matrix but do not propagate into tungsten fibers. Figure 6(c) is a magnified SEM micrograph of the dotted circled area in Figure 6(a). Cracks initiate at tungsten fibers located near the edge of the tensile specimen. The LM2 composite does not show the abrupt fracture as in typical amorphous alloys, but it shows somewhat stable fracture propagation behavior. When the crack initiated at the tungsten fiber meets with the amorphous matrix, it forms multiple shear bands in the matrix. Inside fibers, the crack proceeds in a zigzag pattern as it stops propagating when it meets with longitudinal (tungsten fiber direction) cracks present in fibers as indicated by arrows. Figure 6(d) is a magnified SEM micrograph of the dotted rectangular area in Figure 6(c). Inside the matrix, multiple shear bands are formed, while β dendrites are visible. One of the shear bands is deepened, and the crack propagates along this deepened shear band. Figure 6(e) shows a fractured surface. It is vertical to the tensile direction, and fiber

Table II. Tensile and Compressive Test Results of Zr-Based LM1 and LM2 Amorphous Alloys, Tungsten Fiber, and Tungsten-Fiber-Reinforced Zr-Based LM1 and LM2 Alloy Matrix Composites

Material	Loading Mode	Yield Strength (MPa)	Ultimate Strength (MPa)	Plastic Strain (pct)	Elastic Modulus (GPa)
LM1 alloy*	tensile	956	956	~0	95
	compressive	1920	1943	0.2	91
LM2 alloy	tensile	927 ± 37	927 ± 37	~0	92 ± 2
	compressive	1554 ± 8	1801 ± 13	5.4 ± 0.3	89 ± 2
Tungsten fiber*	tensile	2395	2395	~0	411
LM1 composite*	tensile	1239	1239	~0	169
	compressive	2258	2477	1.5	167
LM2 composite	tensile	1453 ± 16	1456 ± 18	0.03 ± 0.01	195 ± 4
	compressive	2236 ± 7	2432 ± 15	16.4 ± 0.4	189 ± 3

*Tensile and compressive test data were obtained from Lee *et al*[22].

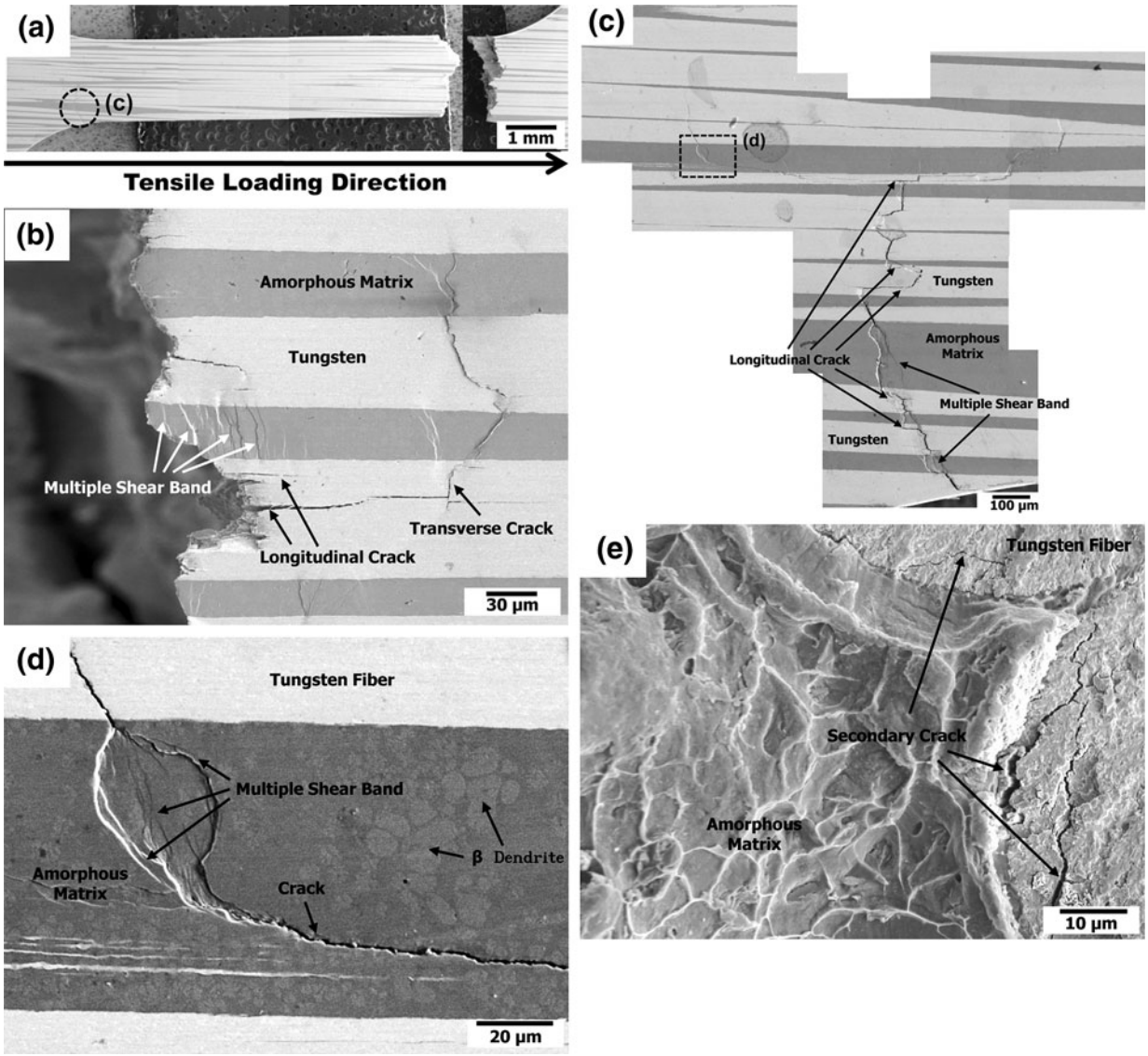

Fig. 6—(*a* through *d*) SEM micrographs of the side region and (*e*) SEM fractograph of the fractured tensile specimen of the tungsten-fiber-reinforced LM2 composite.

pullout or fiber/matrix interfacial debonding frequently observed in typical fiber-reinforced matrix composites is hardly observed. This observation indicates that tungsten fibers are sufficiently constrained by the amorphous matrix and that the bonding between fibers and matrix is quite excellent. The fracture surface consists of vein patterns in the matrix region and cleavage facets in the tungsten fiber region. A few secondary cracks are shown at tungsten fibers and fiber/matrix interfaces as marked by arrows.

C. *Compressive Properties of Tungsten-Fiber-Reinforced Composite*

Figure 5(b) shows compressive stress–strain curves of the LM2 alloy and LM2 composite, and their yield compressive strength, maximum compressive strength, and elongation are summarized in Table II. The yield and maximum compressive strengths of the LM2 alloy are 1554 and 1801 MPa, respectively, and the elongation is 5.4 pct. The yield and maximum strength of the LM2 composite are 2236 and 2432 MPa, respectively, which are approximately 40 pct higher than that of the LM2 alloy. The LM2 composite shows the yielding phenomenon, and its plastic strain is 16.4 pct. The fracture takes place after reaching the maximum strength as the compressive load sustained by fibers decreases. The maximum strength is approximately twice higher than the ultimate strength under tensile loading. It is generally reported that very fine pores and crystalline phases are present inside cast amorphous alloys or their composites.[18,29] They readily develop into voids or cracks under tensile loading and lead to fracture at a lower stress than the maximum compressive strength, whereas they hardly affect compressive properties.[30] When the LM2 composite is compared with the LM1 composite, the plastic strain in the LM2 composite is

much higher (16.4 *vs* 1.5 pct), whereas the strengths similar in the both composites (Table II).[22]

Figures 7(a) through (c) show SEM micrographs of the side region and fractograph of the compressively deformed specimen of the LM2 composite. The fracture proceeds along the compressive loading direction, unlike in typical amorphous alloys where fracture occurs at the maximum shear stress direction (approximately 50 deg angle to the compressive loading direction) (Figure 7(a)). Tungsten fibers undergo slow cracking and fracture, instead of abrupt fracture at one time, because fibers work to withstand the applied load even after reaching the maximum strength, thereby showing a considerable amount of ductility. Longitudinal cracks along the compressive loading direction (or tungsten fiber direction) are observed inside fibers, and some fibers are buckled while sustaining the load. Figure 7(b) is a magnified SEM micrograph of the dotted rectangular area in Figure 7(a). A crack initiates longitudinally at tungsten fibers located inside the tensile specimen, although the matrix is not cracked. Inside the matrix containing β dendrites, multiple shear bands are formed but do not penetrate into β dendrites. Figure 7(c) shows the surface artificially fractured along the dotted line in Figure 7(a). The fracture surface contains vein patterns in the matrix region and cleavage facets of tungsten fibers.

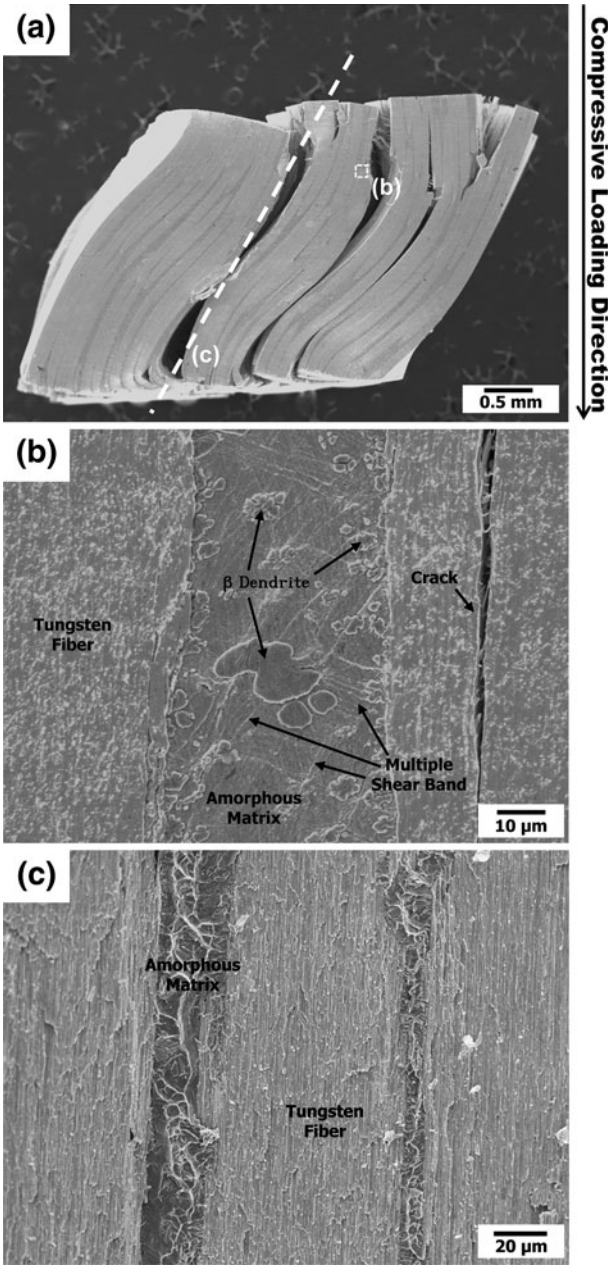

Fig. 7—(*a* through *c*) SEM micrographs of the side region of the compressively deformed specimen of the tungsten-fiber-reinforced LM2 composite.

Figures 8(a) through (c) are SEM micrographs of the cross-sectional area of the compressively deformed specimen of the LM2 composite. Longitudinal cracks along the compressive loading direction are observed inside fibers (marked by arrows), and some fibers are buckled while sustaining the applied load (Figure 8(a)). Figure 8(b) is a magnified SEM micrograph of the dotted rectangular area in Figure 8(a). Most of cracks initiate and propagate longitudinally inside tungsten fibers, whereas a few cracks are found inside the matrix. Figure 8(c) is an example showing a crack propagated from the tungsten fiber into the matrix. Here, the fiber/matrix interfacial separation is not observable, which indicates the strong fiber/matrix interfacial bonding.

IV. DISCUSSION

Because the pressure applied in the current liquid pressing process was higher than the theoretical pressure required for infiltration, the amorphous melt sufficiently infiltrated into the preform of tungsten fibers, and pores formed by solidification or contraction were effectively eliminated. The crystallization caused by the diffusion from tungsten to the matrix or caused by tungsten/matrix interfacial reaction did not occur as other crystalline phases, except β dendrites were not formed in the amorphous matrix (Figure 4(b)). This is related with the high thermal stability of tungsten fibers (melting temperature = 3643 K [3370 °C]). In addition, the DSC analysis data of Figure 3 indicates that the glass transition temperatures (T_g) and crystallization temperatures (T_x) are similar in the LM2 alloy and LM2 composite, which implies that the amorphous matrix is soundly formed during the liquid pressing process.

The compressive strengths of LM1 and LM2 composites are close, whereas there is a significant difference between their tensile strengths. This is because deformation and fracture mechanisms are different under tensile and compressive loading conditions. In fact, it is known that brittle materials such as ceramics show severe anisotropic properties under tensile and compressive loading conditions,[31,32] and amorphous alloys and their composites also have similar anisotropic properties because they have quite brittle characteristics. These problems can be solved by fabricating fiber-reinforced composites whose fiber/matrix bonding strengths are quite high, as in the current tungsten-fiber-reinforced composites.

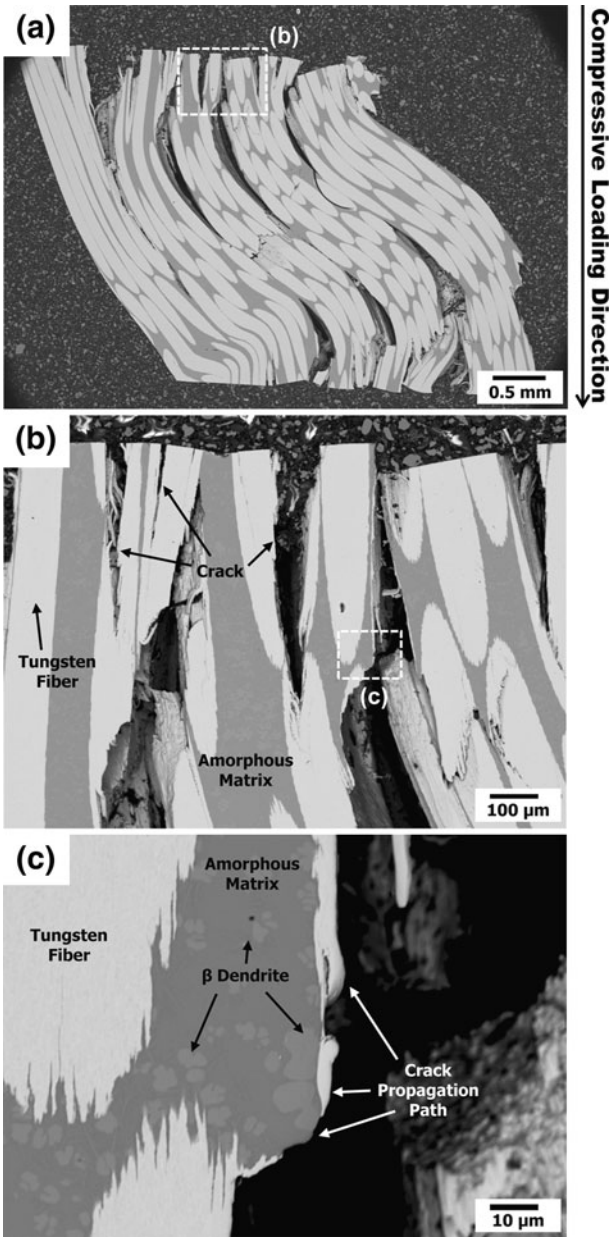

Fig. 8—(*a* through *c*) SEM micrographs of the cross-sectional area of the compressively deformed specimen of the tungsten-fiber-reinforced LM2 composite.

According to the reinforcement of tungsten fibers with much higher strength and elastic modulus than those of the LM2 alloy, the tensile strength and elastic modulus of the LM2 composite are greatly improved by approximately 60 pct and 120 pct, respectively, over the LM2 alloy (Table II). Tungsten fibers do not contribute the improvement of tensile ductility of the LM2 composite because they hardly show the tensile elongation. However, the brittle fracture of the amorphous matrix along the maximum shear stress direction is constrained by tungsten fibers, and the fracture proceeds almost perpendicular to the tensile direction as shown in Figures 6(a) and (b). When cracks initiated at tungsten fibers meet with the amorphous matrix, multiple shear bands are formed in the matrix. Inside tungsten fibers, cracks stop propagating when they meet with longitudinal cracks (tungsten fiber direction) and change their path abruptly at an almost 90 deg angle, thereby showing the zigzag-type propagation path (Figures 6(a) and (c)). This is because cleavage planes of tungsten fibers with a bcc structure are {100} planes consuming the least plastic energy at the crack initiation.[33,34] Thus, the LM2 composite shows somewhat stable fracture propagation behavior, and secondary cracks are observable on the tensile fracture surface (Figure 6(e)).

Under the compressive loading condition, the tungsten-fiber-reinforced LM2 composite shows the plastic strain of 16.4 pct, although the plastic strain of the LM2 alloy is small at 5.4 pct. This is because tungsten fibers show some plastic deformation such as buckling and work to withstand a considerable amount of applied compressive loads, whereas the amorphous matrix is also deformed by forming multiple shear bands (Figure 7(b)). As shown in the compressive stress–strain curve of Figure 5(b), the compressive stress maintains 2230 to 2430 MPa after the yield compressive stress point by the plastic deformation of fibers. This stress–strain behavior is associated with the quite strong fiber/matrix interfaces. Inside tungsten fibers, longitudinal cracks are formed along the compressive loading direction (Figure 8(b)). These cracks lie on {100} planes of tungsten fibers, and some fibers are buckled while sustaining the load. During the compressive test of the composite, the amorphous matrix plays an important role in improving the ductility by deforming with tungsten fibers, by interrupting the propagation of cracks initiated at tungsten fibers, and by taking over a considerable amount of compressive loads while fibers are buckled. In addition, the strong fiber/matrix bonding strength and the increased elongation improve the compressive strength of the composite over the LM2 alloy by approximately 35 pct.

It is interesting to note that the LM2 composite has the higher strength and ductility under tensile and compressive loading conditions than the LM1 composite (Table I). When the monolithic LM1 alloy is compared with the LM2 alloy containing ductile β dendrites, the former has the higher strength and lower ductility than the latter. Thus, the lower strength and higher ductility are expected in the LM2 alloy matrix composite reinforced with tungsten fibers, but both higher strength and ductility result. The higher ductility in the LM2 composite can be explained by the containment of ductile β dendrites in the LM2 composite matrix as dendrites positively affect the ductility, whereas the LM1 composite matrix consists of only amorphous phases. The higher strength in the LM2 composite than in the LM1 composite is not easily explained because the higher elongation generally results in the higher strength. In view of strength and ductility, the difference in tensile and compressive deformation behavior needs to be investigated in detail.

In the initial tensile deformation stage of the LM2 composite, cracks initiate at tungsten fibers, whereas cracks initiate at the amorphous matrix and propagate in a shear fracture mode while the shear fracture is constrained by fibers in the LM1 composite.[22] In the

LM2 composite, thus, the crack propagation proceeds relatively slow as the amorphous matrix containing ductile β dendrites plays a role in interrupting the crack propagation path in a zigzag pattern by forming multiple shear bands inside, thereby showing some tensile plastic strain, whereas the tensile elongation is nil in the LM1 composite. Because the LM2 composite is fractured in the plastic region, the strength increases sufficiently with increasing tensile strain. In the LM1 composite, however, the strength cannot increase sufficiently, and the fracture occurs within the elastic strain region, which leads to the lower strength than that of the LM2 composite. It is interesting that the amorphous matrix and tungsten fibers hardly show any plastic strains, but when they are combined, the composite shows some plastic strain. These distinctive tensile properties of the LM2 composite show a synergy effect arising from the mixing of amorphous matrix and tungsten fibers. The ultimate tensile strength reaches 1456 MPa as the composite is strained up to the plastic region.

This simultaneous improvement of strength and ductility in the LM2 composite over the LM1 composite is clearly visible in the compressive test data. The plastic strain of the LM2 composite is ten times higher than that of the LM1 composite, whereas the strength level is similar in both composites. This result is attributed to some plastic deformation of tungsten fibers and the formation of multiple shear bands in the matrix under compressive loading.[23] Cracks initiate longitudinally along the compressive loading direction because these cracks lie on {100} planes of tungsten fibers, but some fibers are buckled. The amorphous matrix interrupts the radical propagation of cracks initiated at tungsten fibers, and it is deformed with tungsten fibers by forming multiple shear bands. On the contrary, in the LM1 composite, cracks initiate in the amorphous matrix at the maximum shear stress direction, and most of the tungsten fibers are broken by shear cracks initiated and propagated from the amorphous matrix while some fibers work to withstand the applied load, thereby showing only a small amount of ductility (1.5 pct). It is also noted that the improvement in compressive plastic strain of the LM2 composite is more visible than that of fibers and LM2 alloy matrix themselves. This improvement occurs because merits of both fibers and amorphous matrix are well taken into advantage as multiple shear bands formed in the amorphous matrix, whereas buckling in fibers occurs because of the excellent bonding of interfaces between the fibers and matrix.[30]

Based on the findings of this study on tungsten-fiber-reinforced LM2 amorphous matrix composite fabricated by the liquid pressing process, the strength, elastic modulus, and ductility of the LM2 composite can be improved over the LM2 alloy and the tungsten-fiber-reinforced LM1 amorphous matrix composite under both tensile and compressive loading conditions while maintaining advantages of strong tungsten fibers and amorphous alloys. This enhanced strength, elastic modulus, and ductility can be explained by the presence of fibers in terms of mechanisms such as (1) interrupted propagation of cracks initiated in tungsten fibers, (2) the formation of lots of multiple shear bands in the amorphous matrix, and (3) sharing of loads and deformation of tungsten fibers and amorphous matrix because of the excellent bonding of interfaces between them. This outstanding result was unreported in previous studies on amorphous matrix composites. Because only Zr-based amorphous composites reinforced with tungsten fibers are compared in this study, the microstructures of various amorphous composites fabricated under various chemical compositions and reinforcements are to be analyzed, and more fundamental correlation study between microstructures and deformation mechanisms is to be investigated in the future.

V. CONCLUSIONS

The LM2 alloy matrix composite reinforced with tungsten fibers was fabricated by the liquid pressing process, and its tensile and compressive properties were examined in relation with microstructures and deformation mechanisms.

1. The LM2 composite with strong fiber/matrix interfaces was successfully fabricated without pores and misinfiltration by the liquid pressing of tungsten fibers and LM2 alloy. Overall, 68 vol pct of tungsten fibers was distributed in the matrix, in which 35 vol pct of ductile β dendrites were present. Other crystalline phases were hardly found as the crystallization did not occur because of the high thermal stability of tungsten fibers.
2. According to the reinforcement of tungsten fibers with very high strength and elastic modulus, the tensile strength and elastic modulus of the LM2 composite were greatly improved over the LM2 alloy, whereas tungsten fibers did not contribute the improvement of tensile ductility. Shear fracture of the amorphous matrix was constrained by fibers, and fracture proceeded almost perpendicular to the tensile direction. Thus, the LM2 composite showed somewhat stable crack propagation behavior as cracks stopped propagating when they met with longitudinal cracks of tungsten fibers and amorphous matrix containing ductile β dendrites.
3. According to the compressive test results of the LM2 composite, fracture did not take place at one time after the yield point, but it proceeded as the loading was sustained by fibers, thereby leading to the maximum strength of 2432 MPa and plastic strain of 16.4 pct. During the compressive deformation, the amorphous matrix worked for improving the ductility by deforming with tungsten fibers, by interrupting the propagation of cracks initiated at tungsten fibers, and by taking over a considerable amount of compressive loads while fibers were buckled.
4. Even though the amorphous matrix and tungsten fibers hardly showed any plastic strains, the LM2 composite showed some plastic strain, and thus, the LM2 composite had the higher strength, elastic

modulus, and ductility under both tensile and compressive loading conditions than the LM1 composite. These distinctively excellent properties indicated a synergy effect arising from the mixing of amorphous matrix and tungsten fibers and the excellent bonding of interfaces between them.

ACKNOWLEDGMENTS

This work was supported by the National Research Foundation of Korea (NRF) grant funded by the Korean Ministry of Education, Science, and Technology (No. 2010-0026981). The authors are grateful to Drs. Young Buem Song of Agency for Defense Development and Choongnyun Paul Kim of POSTECH for their helpful discussion on the fabrication of the composites.

REFERENCES

1. L.-Q. Xing, Y. Li, K.T. Ramesh, J. Li, and T.C. Hufnagel: *Phys. Rev. B*, 2001, vol. 64, pp. 180201(R)-4.
2. J.G. Lee, D-G. Lee, S. Lee, and N.J. Kim: *Metall. Mater. Trans. A*, 2004, vol. 35A, pp. 3753–61.
3. T.G. Nieh, C. Schuh, J. Wadsworth, and Y. Li: *Intermetallics*, 2002, vol. 10, pp. 1177–82.
4. W.J. Wright, R. Saha, and W.D. Nix: *Mater. Trans.*, 2001, vol. 42, pp. 642–49.
5. A. Inoue, W. Zhang, T. Zhang, and K. Kurasaka: *Acta Mater.*, 2001, vol. 49, pp. 2645–52.
6. Z.F. Zhang, J. Eckert, and L. Schultz: *Acta Mater.*, 2003, vol. 51, pp. 1167–79.
7. S. Gonzalez, J. Sort, D.V. Louzquine-Luzgin, J.H. Perepezko, M.D. Baro, and A. Inoue: *Intermetallics*, 2010, vol. 18, pp. 2377–84.
8. R.D. Corner, R.B. Dandliker, and W.L. Johnson: *Acta Mater.*, 1998, vol. 46, pp. 6089–6102.
9. P. Wadhwa, J. Heinrich, and R. Busch: *Scripta Mater.*, 2006, vol. 56, pp. 73–76.
10. C. Fan, C. Li, A. Inoue, and V. Haas: *Phys. Rev. B*, 2000, vol. 61B, pp. R3761–63.
11. H.T. Jeong, W. Yook, B.J. Kim, W.T. Kim, and D.H. Kim: *Metall. Mater. Int.*, 2010, vol. 16, pp. 517–22.
12. H. Choi-Yim, R. Busch, U. Koster, and W.L. Johnson: *Acta Mater.*, 1999, vol. 47, pp. 2455–62.
13. M. Tavoosi, M.H. Enayati, and F. Karimzadeh: *Metall. Mater. Int.*, 2011, vol. 17, pp. 853–56.
14. Y.K. Xu, H. Ma, J. Xu, and E. Ma: *Acta Mater.*, 2005, vol. 53, pp. 1857–66.
15. M.H. Lee, J.Y. Lee, D.H. Bae, W.T. Kim, D.J. Sordelet, and D.H. Kim: *Intermetallics*, 2004, vol. 12, pp. 1133–37.
16. K.-Y. Kim, H.-S. Joo, B.-H. Kang, and W. Gao: *Metall. Mater. Int.*, 2011, vol. 17, pp. 857–63.
17. H.-S. Chin, J.-Y. Suh, K.-W. Park, W. Lee, and E. Fleury: *Metall. Mater. Int.*, 2011, vol. 17, pp. 541–45.
18. F. Szuecs, C.P. Kim, and W.L. Johnson: *Acta Mater.*, 2001, vol. 49, pp. 1507–13.
19. C.C. Hays, C.P. Kim, and W.L. Johnson: *Mater. Sci. Eng. A*, 2001, vol. 304, pp. 650–55.
20. Y.H. Jang, S.S. Kim, S.K. Lee, D.H. Kim, and M.K. Um: *Compos. Sci. Technol.*, 2005, vol. 65, pp. 781–84.
21. S.B. Lee, K. Matsunaga, Y. Ikuhara, and S.K. Lee: *Mater. Sci. Eng. A*, 2007, vols. A449–51, pp. 778–81.
22. K. Lee, S.-B. Lee, S.-K. Lee, and S. Lee: *Metall. Mater. Trans. A*, 2008, vol. 39A, pp. 1319–26.
23. K.Q. Qui, A.M. Wang, H.F. Zhang, B.Z. Ding, and Z.Q. Hu: *Intermetallics*, 2002, vol. 10, pp. 1283–88.
24. B. Clausen, S.Y. Lee, E. Ustundag, C.C. Aydiner, R.D. Conner, and M.A.M. Bourke: *Scripta Mater.*, 2003, vol. 49, pp. 123–28.
25. I.N. Jujur and S. Hanada: *Mater. Sci. Eng. A*, 1995, vol. 192, pp. 848–55.
26. M. Nishida, T. Hanabusa, Y. Ikeuchi, and N. Minakawa: *Materialwiss. Werkst.*, 2003, vol. 34, pp. 49–55.
27. C.C. Hays, C.P. Kim, and W.L. Johnson: *Phys. Rev. Lett.*, 2001, vol. 84, pp. 2901–04.
28. Y.L. Huang, A. Bracchi, T. Niermann, M. Seibt, D. Danilov, B. Nestler, and S. Schneider: *Scripta Mater.*, 2005, vol. 53, pp. 93–97.
29. J.W. Qiao, Y. Zhang, and G.L. Chen: *Mater. Des.*, 2009, vol. 30, pp. 3966–71.
30. J.L. Walter and C.L. Briant: *J. Mater. Res.*, 1990, vol. 5, pp. 2004–22.
31. V.R. Mastelaro and E.D. Zanotto: *J. Non-Cryst. Solids*, 1999, vol. 247, pp. 79–86.
32. R.S. Kottada and A.H. Chokshi: *Acta Mater.*, 2000, vol. 48, pp. 3905–15.
33. D. Dragoi, E. Üstündag, B. Clausen, and M.A.M. Bourke: *Scripta Mater.*, 2001, vol. 45, pp. 245–52.
34. C.R. Krenn, D. Roundy, J.W. Morris, and M.L. Cohen: *Mater. Sci. Eng. A*, 2001, vols. A319–21, pp. 111–14.